ADVANCED MATERIALS

DOI: 10.1002/adma.200701527

Superelasticity and Shape Memory in Micro- and Nanometer-scale Pillars**

By *Jose M. San Juan*,* *Maria L. Nó*, and *Christopher A. Schuh*

Micro- and nanoelectromechanical systems (MEMS and NEMS, respectively) are being developed intensively and constitute a new paradigm of technological development for the present century. With a growing world-wide market in excess of one hundred billion dollars, MEMS and NEMS pose a challenge for the science and technology of microfabrication[1] and have already found usage as sensors and actuators across numerous industrial sectors,[2] from automotive, aerospace, and telecommunications[3] to emerging biomedical technologies.[4] In parallel, the development of multifunctional and smart materials[5] is converging with miniaturization technologies, enabling a new generation of smart MEMS (SMEMS). Among the different smart materials targeted for use in SMEMS, shape memory alloys have attracted considerable interest[6,7] because they offer the highest output work density (about 10^7 J m^{-3}), and exhibit specific desirable thermomechanical effects owing to the reversibility of their thermoelastic martensitic transformation.[8] In particular, integrating into MEMS components that exhibit superelasticity, or one-way or two-way shape memory, would enable a new generation of functional microdevices. In the last decade, great effort has been devoted to the production of shape memory thin films, which could be integrated into the planar technology of microsystems. Shape memory thin films have been mainly produced by sputtering, and exhibit both superelastic and shape memory properties. The effort has largely been focused on the Ti-Ni system (reviewed by Miyazaki and Ishida[9]), and combinatorial methods are also being applied to develop new compositions not presently used in bulk shape memory applications.[10] However, although such sputtered films are often made with thicknesses between 0.5 and 15 μm, the desirable thermomechanical effects of superelasticity and shape memory have only been tested and exploited for applications using their largest dimensions above millimeter size.[6,7,9] Thus, there remain important unanswered questions about the nature of these thermomechanical effects at the scales relevant to MEMS and NEMS applications. In the present work the first objective is to design and produce simple shape memory alloy features of micro- and nanometer-scale dimensions, smaller in every dimension than a typical thin film thickness currently obtained by sputtering–around 5 μm. The second objective is to demonstrate on such features the thermomechanical properties of superelasticity and shape memory at the nanometer scale. We report that stress-induced or thermal martensitic transformation can take place at the nanometer scale in a reversible way; individual martensite variants below 25 nm thick appear in these experiments. The presented results demonstrate that in Cu-Al-Ni shape memory alloys, completely recoverable superelasticity, in a high number of cycles, is achievable at the very fine scales pertinent to MEMS devices.

From a practical perspective, a first issue to consider is how we can demonstrate and quantify shape memory and superelastic properties at very small feature scales. One possible approach relies on nanoindentation techniques,[11] which in the last decade have been plied to address fundamental issues of deformation in a broad range of materials (see a review by Schuh[12]). Recently, nanoindentation techniques have been successfully applied to shape memory alloys, both as thin films and bulk materials.[13–15] However, the complex multiaxial nature of deformation around a nanoindenter renders interpretation of the data very difficult, especially for shape memory materials where there are complex thermal or stress induced phase transformations that are responsive to details of the loading state. Nanoindentation results are therefore very difficult to extrapolate to desirable geometries and loading states for MEMS and NEMS components.

A second, more fundamental issue, concerns the minimum size at which the martensitic transformation can be induced. For example, some works indicate that in the most common shape memory alloy, Ti-Ni, the martensitic transformation is suppressed for grains below 60 nm diameter[16] and for films of 50 nm thickness.[17] However, in a different alloy, Cu-Al-Ni, some of the present authors have recently shown, by carrying out in situ tests in the transmission electron microscope,[18,19] that the thermal or stress-induced martensitic transformation takes place in regions below 50 nm thickness,

[*] Prof. J. San Juan,[+] Prof. C. A. Schuh
Department of Materials Science and Engineering
Massachusetts Institute of Technology
77 Massachusetts Avenue, Cambridge, MA 02139 (USA)
E-mail: sanjuan@mit.edu
Prof. M. L. Nó
Department of Applied Physics II
Universidad del Pais Vasco
Box 644, Bilbao, 48080 (Spain)
[+] Current address: Department of Physics of Condensed Matter, Universidad del Pais Vasco, Box 644, Bilbao, 48080, Spain.

[**] J.S.J. thanks the University of the Basque Country and the Spanish Ministry of Science and Education, for the Sabbatical license and the Mobility Grant to stay at MIT. This work was supported by the project MAT2004-03166, from the Spanish Ministry of Science and Education, and the ETORTEK-ACTIMAT-05 project of the Basque Government. C.A.S. acknowledges the support of the US Office of Naval Research, grant N00014-04-1-0669.

and the nucleation and progress of martensite variants as small as 20 nm has been observed. These results suggest that the desirable properties of shape memory and superelasticity may be possible on the scale of MEMS and even NEMS devices, but a simultaneous demonstration of both properties in a specimen of such dimensions has yet to be presented. It is the goal of this Communication to provide such a demonstration.

To avoid the influence of microstructure in this study, we have used [001] oriented single crystals of a Cu-Al-Ni shape memory alloy, whose transformation temperatures were studied previously.[20] Two samples with different compositions were used for the present study. The first one with a Cu-14Al-4Ni (wt %) composition exhibits transformation temperatures of M_s = 252 K, M_f = 242 K, A_s = 273 K, and A_f = 285 K (corresponding to martensite start and finish and austenite start and finish, respectively). We have chosen this sample, called hereafter SE, for the superelastic tests, because at room temperature it is in its high temperature phase (austenite), and consequently the transformation to martensite can be induced by stress. The second sample, with composition Cu-13.7Al-5Ni (wt %), transforms at M_s = 291 K, M_f=273 K, A_s = 285 K, and A_f = 303 K. We have chosen this sample, called hereafter SM, for the shape memory tests, because at room temperature it can be in the austenite phase when cooling from high temperature, or partially in martensite if it has been previously transformed.

The simplest features we can consider in order to test the thermomechanical properties under simple loading conditions, are micropillars produced by focused ion beam (FIB) micromachining. Such pillars were recently successfully used to test the influence of sample dimensions on crystal plasticity in conventional metals and alloys,[21,22] and are readily adapted to study shape memory alloys. We used FIB to micromachine [001] oriented cylindrical pillars from the surface of thin sections cut from bulk Cu-Al-Ni single crystals. Microcompression tests were performed by instrumented nanoindentation with a Triboindenter (from Hysitron, Inc.) and a sphero-conical diamond indenter tip of 0.6 μm radius. This equipment allows constant force contact-mode images to be obtained by means of a piezoelectric scanning system, which is very useful to precisely position the indenter tip over the pillar.

We first describe the superelastic tests performed on sample SE. Figure 1a shows one of the micro-pillars machined by FIB, with 5.1 μm height and 1.7 μm diameter, giving an aspect ratio near three as recommended for micro-compression tests.[23]

After carefully positioning the apex of the indenter over the pillar, we carried out a multiple-cycle compression test: two cycles were applied with a maximum load of 500 μN, followed by two cycles at 750 μN, and finally two at 1000 μN. The results from these tests, load versus displacement, are plotted in Figure 1b, in which we show for clarity only cycles 1, 3, 5, and 6. The curves show clearly that at a load of about 425–450 μN, a sudden high strain plateau occurs, in which more than

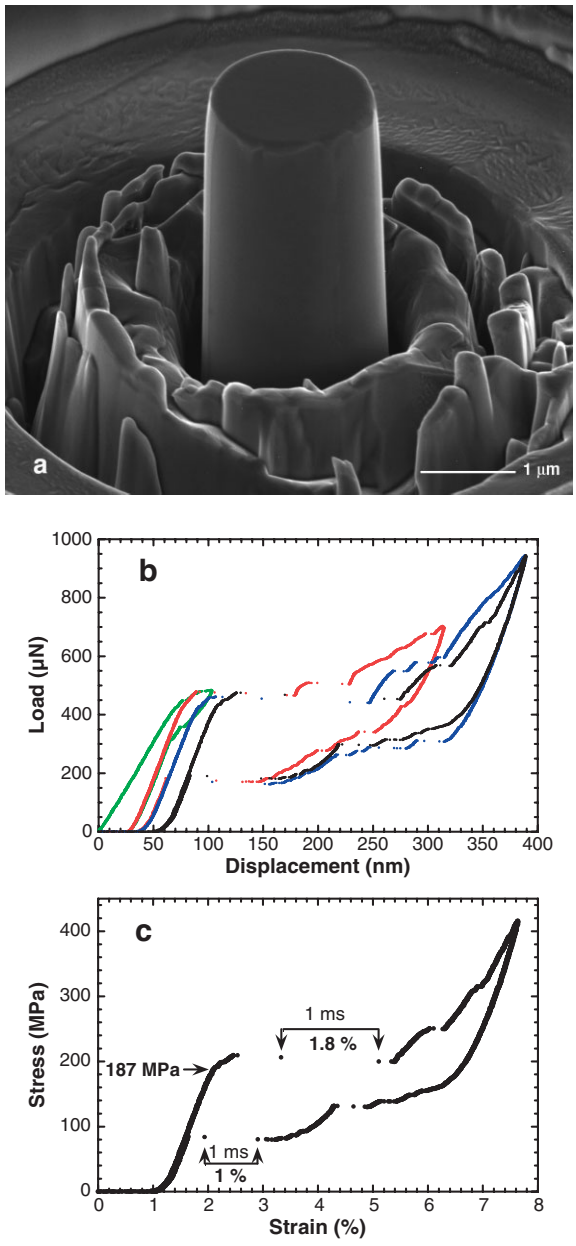

Figure 1. Superelastic behavior of micropillars. a) Image of a [001] Cu-Al-Ni oriented micropillar in sample SE. b) Superelastic cycles measured by microcompression of the micropillar shown in (a). c) Stress-strain curve obtained from the sixth superelastic cycle of (b).

100 nm of travel are accommodated with relatively little increase in the applied load. For comparison, we note that the pop-in events due to dislocation motion during incipient plasticity have a much smaller typical depth of just a few nanometers.[24] At higher strains there is a steepening of the load-displacement response until the maximum load is reached. During unloading the apparent penetration depth is recovered (albeit with hysteresis), and for loads below about 185 μN the curve follows the elastic loading slope. During the first cycle at any given maximum load (cycles 1 in green, 3 in

ADVANCED MATERIALS

red and 5 in blue) there is a small amount of un-recovered displacement due to settling of the indenter; subsequent cycles at the same load lead to ideal overlap of the elastic portions of the curves (cf. cycles 5 and 6, in blue and black, respectively). More details on this unrecovered "settling" strain are provided in the experimental section, a main conclusion being that beyond the first load cycle, the micro-pillar experiences essentially uniform compressive strain. The load-displacement behavior seen in Figure 1b is a demonstration of the superelastic effect in the sample SE. At 425 μN the martensitic transformation is induced by the applied stress, giving rise to a large compressive transformation strain. These raw data can also be converted into conventional stress-strain curves, as shown in Figure 1c, allowing us to identify the critical stress σ_c for the stress-induced martensitic transformation. Based on Figure 1c, we find $\sigma_c \approx 187$ MPa, which agrees to within ± 18 MPa with the values measured in compression tests on bulk single crystals of similar composition.[25] In addition, we can calculate from Figure 1c the uniaxial elastic modulus along the [001] direction, E[001] = 22.5 GPa, which also agrees with the corresponding modulus measured in bulk Cu-Al-Ni oriented single crystals of similar composition, E[001] = 23.5 GPa.[26]

Another interesting point to be remarked upon in Figure 1c concerns the transformation speed during the stress plateaus upon loading and unloading. These microcompression experiments have millisecond resolution, and during the phase transformation a substantial amount of strain can accumulate in that time interval. Along the stress plateau in Figure 1c, two successive points are marked, corresponding to a compression strain of 1.8 %. Similarly, the two points marked during unloading are also spaced 1 ms in time, with a recovered strain of 1.0 %. From these values we expect that SMEMS exploiting the superelastic effect at the nanometer scale, even using up to 3 % strain, could operate at frequencies as high as 1 KHz. This is well above the 100 Hz reported up to now in the literature for thin film devices.[27,28]

We have also performed microcompression tests comprising many dozens of cycles to above 5 % strain on similar micro-pillars, with complete superelastic recovery. As an example, we present in Figure 2 two consecutive superelastic cycles in another slightly smaller micro-pillar (1.6 μm diameter), after superelastic cycling for more than one hundred cycles; the stability and reproducibility of the superelastic effect are noteworthy.

We now turn to a description of the tests performed on sample SM. Figure 3a shows a micro-pillar of sample SM, with a higher aspect ratio (height 8.4 μm, diameter 1.8 μm) than the previous micro-pillars from sample SE. The experimental procedure was the same as in previous case, but in this case only two successive cycles were performed as shown in Figure 3b. Along the first cycle (in black) two sudden strain steps are observed during loading, and during unloading some recovery is observed, but the sample retains an un-recovered displacement of 300 nm. The second loading cycle (in red) reaches a maximum displacement of 690 nm and after unloading it retains a total residual displacement of 500 nm. With contact-mode images of the pillar before and after loading, we confirmed that most all of the 500 nm residual displacement can be attributed to the compression strain accumulated by the micro-pillar, with no contribution from buckling.

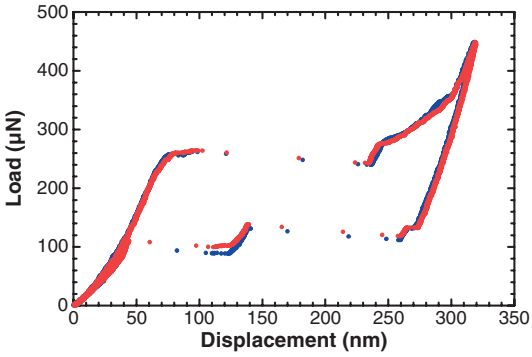

Figure 2. Superelastic cycling reproducibility in micropillars. Two consecutive superelastic cycles, in blue and red, measured after 110 prior loading-unloading cycles, in a micro pillar on sample SE.

In Figure 3b, the microcompression test was performed at room temperature and initially the SM pillar was in the austenite phase. However, once the stress-induced transformation occurred during the first loading cycle, some martensite variants became stable because they were below A_f; only a small amount of reverse transformation occurred. After the second cycle most of the martensite variants were apparently stabilized, and no clear reverse transformation occurred; this accounts for the large residual strain.

After the microcompression test of Figure 3b, we performed an additional experiment on the same micro-pillar, now in the martensitic state. Applying a compression load somewhat off-center of the pillar axis, we induced a lateral bending force on the column. In this configuration, the apex of the indenter glided off of the top of the pillar, and slightly damaged the edge. However, the main deformation induced by this procedure was a bending of the micro-pillar to one side, and because the pillar was in the martensite phase for this test the deformation was not recovered; after the experiment the pillar remained bent, as shown in Figure 3c. Looking closer at the micro-pillar in the bent condition in Figure 3d, we see that the lateral side of the pillar shows a striped pattern of martensite variants, which reoriented to accommodate the flexural strain of the pillar. The thickness of the martensite domains varies from about 100 to less than 25 nm.

After the bending procedure described above, the sample was moderately heated to above A_f, and observed in a scanning electron microscope. The post-heating pictures of Figure 3e and f evidence complete shape recovery of the pillar by the one-way shape memory effect. Obviously, the shape recovery is accompanied by the disappearance of the martensite variants on the pillar surface (compare Fig. 3d after deformation and Fig. 3f after subsequent heating). We know that during one-way shape memory recovery,[8] forces equivalent to

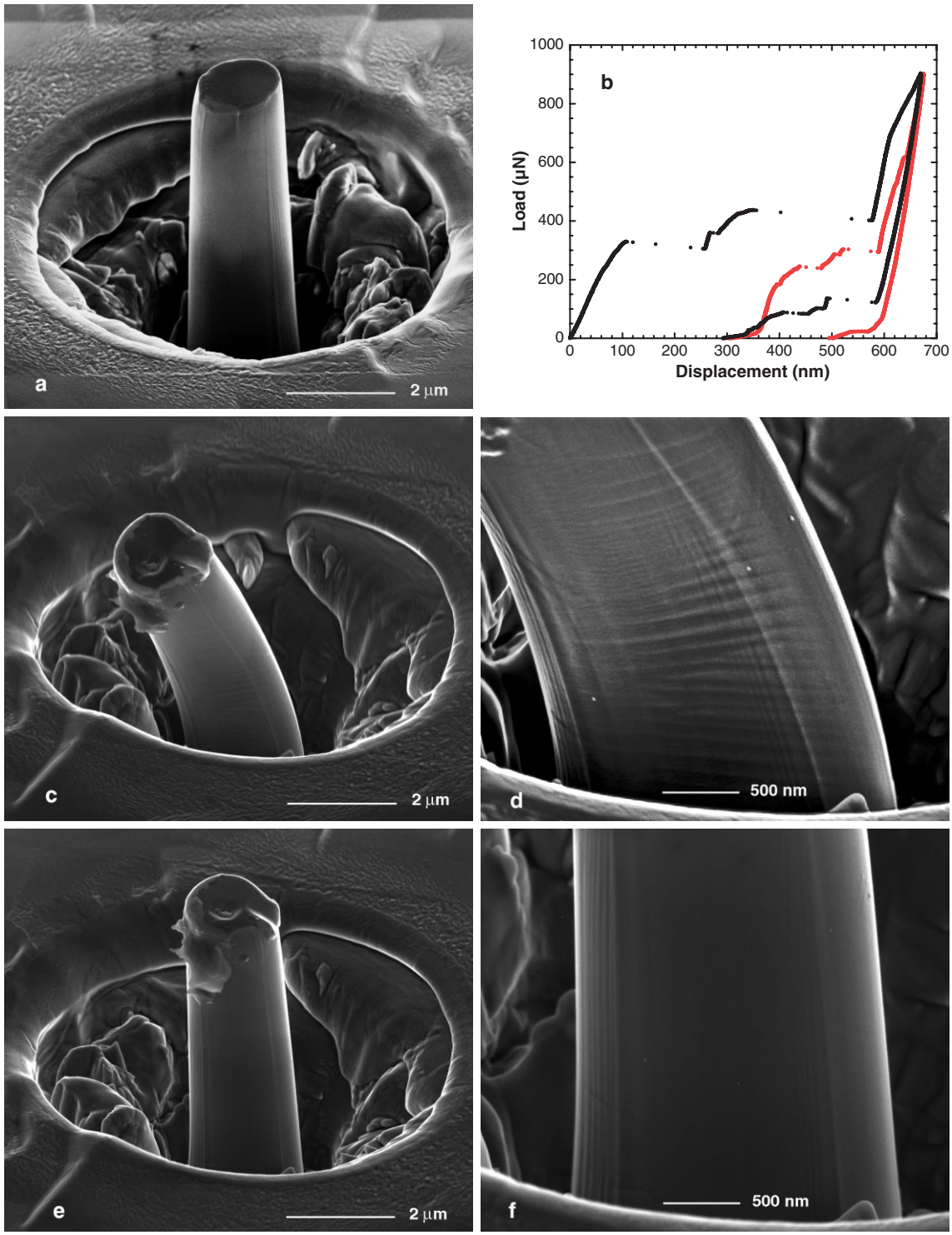

Figure 3. Microcompression tests on a shape memory micropillar before and after deformation and further shape recovery by heating. a) Image of a [001] Cu-Al-Ni oriented micropillar from sample SM, initially in the austenite phase. b) Microcompression load-displacement curves during two loading-unloading cycles. c) Same micropillar as in (a), deformed in bending by the application of off-center loading on the column. d) Detailed view of the nanometer-sized martensite variants accommodating the strain in the bent condition from (c). e) Shape recovery of the same sample, affected by in situ heating. f) Corresponding detailed view of the side of the micropillar showing the disappearance of martensite variants in the recovered state, after heating.

ADVANCED MATERIALS

the stress-induced recovery plateau at the heated temperature are developed. So in the present case forces of some hundreds of μN are expected, which speaks to possibilities for positioning and actuation operations in microdevices.

We have seen this completely-recoverable shape memory behavior not only in super-micrometer-scale pillars such as that in Figure 3, but also in nanometer-scale pillars of as small as ~ 300 nm in diameter. Figure 4a illustrates one such pillar

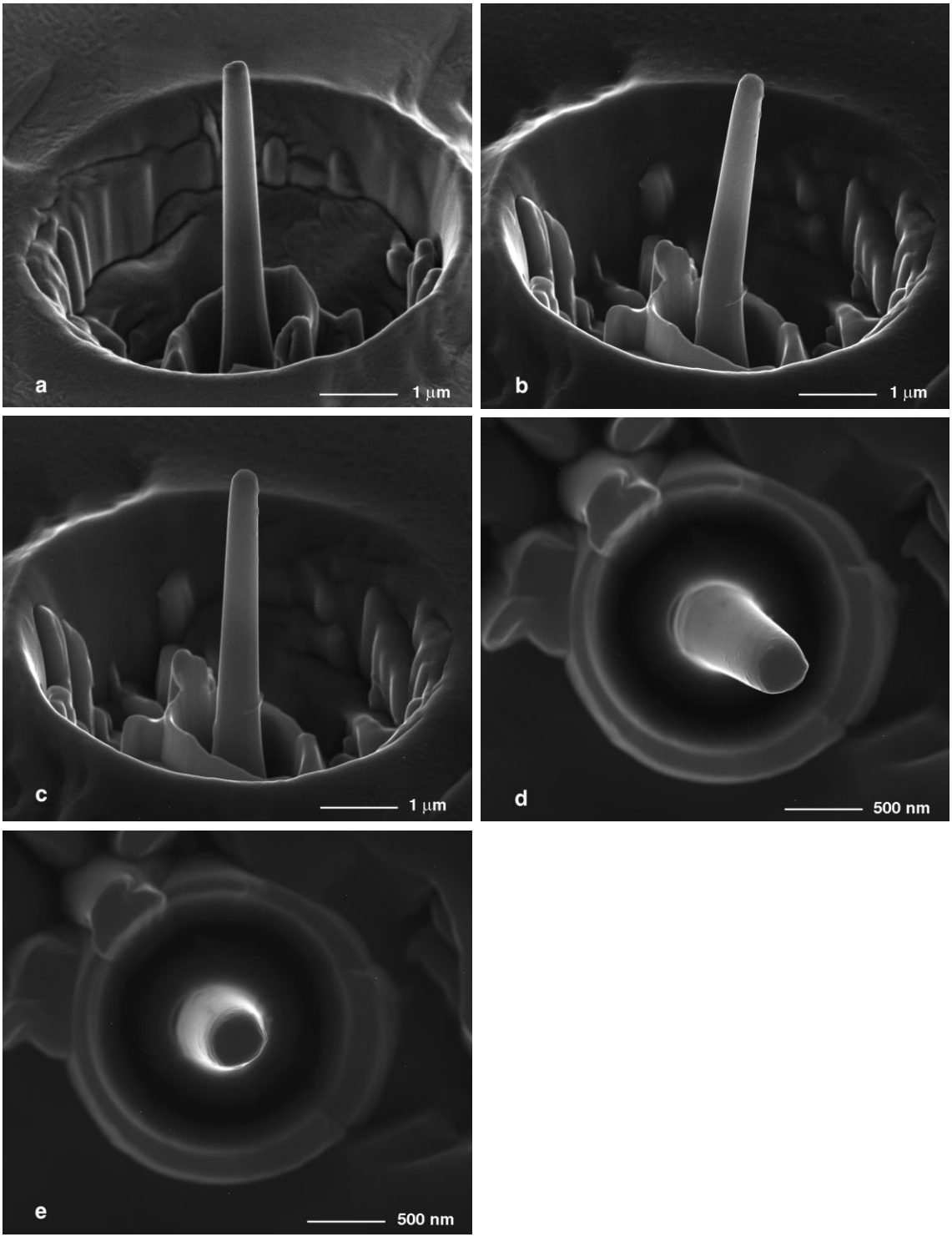

Figure 4. Shape memory nanopillar. a) Image of a nanopillar with ~ 400 nm diameter, from sample SM. b) The same nanopillar deformed in bending. c) Shape recovery of the nanopillar by in situ heating. d,e) Bird's eye views of the specimen in the previous (b) and (c) conditions, respectively.

of 6 μm height with an aspect ratio of about 20. Again in this case we used the tip of the nanoindenter to apply off-axis load and deform the nanopillar in a bending mode, as shown in Figure 4b. By heating to above A_f, we again observed strain recovery by the one-way shape memory effect, as is shown in Figure 4c. The lateral displacement of the nanopillar and its recovery are better observed from the bird's eye views after deformation, Figure 4d, and after heating and recovery, Figure 4e. In these pictures a displacement recovery of 400 nm is measured at the top of the nanometer-scale pillar.

The above results show that in Cu-Al-Ni shape memory alloys, stress-induced or thermal martensitic transformation can take place at the nanometer-scale in a reversible way; individual martensite variants below 25 nm thickness appear in these experiments (Fig. 3d), in good agreement with in situ microscopy observations.[18,19] We believe that previously reported problems for martensite nucleation at this scale[16,17] could in some cases be related to a lack of local crystallinity of the sample, or particularly in the case of Ti-Ni alloys, to local deviations in stoichiometry because of titanium depletion due to oxidation, as proposed to occur in Ti-Ni thin films.[29] Over the course of these experiments, our samples have been continuously stored and tested in air, so it seems that oxidation does not pose special problems for Cu-Al-Ni.

Finally, the presented results demonstrate that in Cu-Al-Ni alloys, completely recoverable superelasticity is achievable at the very fine scales pertinent to MEMS devices. Superelastic cycling over hundreds of nanometers of displacement can be achieved for a high number of cycles. These results suggest the possibility of designing SMEMS with superelastic components operating at frequencies close to 1 KHz, and with strains as high as 3 %. Our results also demonstrate that the one-way shape memory effect operates in Cu-Al-Ni in samples of nanometer-scale dimensions, so devices such as the presented micro- and nanopillars could be designed as thermal sensors and actuators. Recovery forces of several hundred μN are expected to actuate along hundreds of nanometers, paving the way for high-work-output nanoactuators.

Experimental

The micro- and nanometer-scale pillars used in the present work were machined by FIB at the Center for Nanoscale Systems of Harvard University, with a FEI Dual Beam DB235. Each pillar was machined in the center of a double crater, as shown in Supporting Information Figure 1a, which is the same as pictured in Figure 1a in the paper. We oversized the external crater in order to avoid the possibility of contact between the indenter tip and the sides of the crater during the microcompression tests, as reported by some authors [30]. The microcompression tests were performed in a Hysitron Triboindenter in the Nanomechanical Technology Laboratory at MIT, with the following basic procedure.

First, we identified the position of the crater on the sample surface, and used the indenter tip as a scanning probe at a fixed contact load of 2 μN, in order to acquire a contact-mode topography image of the surface. In Supporting Information Figure 1b we show the image corresponding to the micropillar of Supporting Information Figure 1a. Note that in this image, the edge resolution is limited by the conical shape of the indenter tip, but the location of the pillar is still easily identified, and the indenter can be quite precisely positioned with respect to the pillar axis; this is critical to ensure on-axis loading for superelasticity tests, and is also useful to apply off-axis loads and induce bending in the shape memory tests.

In our tests, we have conducted the indenter tip positioning with the following sequence. We first perform a 5×5 μm scan, and follow this with a higher-magnification scan at 3×3 μm centered on the top of the pillar. We acquire the latter image with a very low scan rate of about 3 μm s^{-1}, in order to insure good coincidence between the images acquired during the forward and reverse scans. From the final image, the tip is carefully located at the center of the pillar. Our microcompression tests were conducted with a constant applied force rate of 250 μN s^{-1}.

Supporting Information Figure 1c and d shows a view of the top of a typical micropillar obtained by in situ contact-mode imaging with the tip of the indenter, just before and after the microcompression experiment shown in Figure 1b. Although the top of the micropillar is flat with a sharp lateral edge (see Fig. 1a), these contact mode-images suffer from some imaging artifacts at the sharp edges, which appear rounded in Supporting Information Figure 1c and d. There is a possibility of some dust contamination due to static electricity at the top of the pillar, but we believe that this effect mostly stems from the geometry of the imaging tip; at sharp edges, the image is constructed based on contact with the conical side of the indenter tip, and not by its apex. Away from the edges, the flat surface is clearly revealed because the apex is the imaging contact point.

In order to appreciate the local plastic deformation produced by the tip of the indenter, in Supporting Information Figure 1e we compare the depth profiles from both images (Supporting Information Fig. 1c and d). Apart from the artificial shoulders at the edges, we can see the profile of the remnant penetration depth due to the local plastic deformation produced by the indenter. The maximum residual depth is about 70 nm, which corresponds to the accumulated plastic deformation produced during the first loading cycles at each maximum load, such as can be seen in Figure 1b. For this reason we believe that the "settling" effect described in the paper corresponds to the development of this minor impression on the first cycle at a given maximum load. Beyond the first cycle, the top surface of the pillar is more conformal to the indenter tip, so that the applied load is distributed sufficiently homogeneously over the cross-section of the pillar and a reasonably close approximation to ideal uniaxial loading is achieved.

Received: June 26, 2007
Revised: October 30, 2007
Published online: December 20, 2007

[1] M. J. Madou, *Fundamentals of Microfabrication*, CRC Press, Boca Raton, FL **2002**.
[2] C. Liu, *Fundations of MEMS*, Pearson Prentice-Hall, Upper Saddle River, NJ **2006**.
[3] T. R. Hsu, *MEMS and Microsystems*, McGraw-Hill, Boston, MA **2002**.
[4] *Bio-MEMS* (Eds: W. Wang, S. A. Soper), CRC Press, Boca Raton, FL **2007**.
[5] *Smart Technologies* (Eds: K. Worden,W. A. Bullongh, J. Hayvood), World Scientific, New Jersey, NJ **2003**.
[6] K. Bhattacharya, R. D. James, *Science* **2005**, *307*, 53.
[7] M. Kohl, *Shape Memory Microactuators*, Springer, Berlin **2004**.
[8] *Shape Memory Materials* (Eds: K. Otsuka, C. M. Wayman), Cambridge University Press, Cambridge **1998**.
[9] S. Miyazaki, A. Ishida, *Mater. Sci. Eng. A* **1999**, *273–275*, 106.
[10] J. Cui, Y. S. Chu, O. O. Famodu, Y. Furuya, J. Hattrck-Simpers, R. D. James, A. Ludwing, S. Thienhaus, M. Wuttig, Z. Zhang, I. Takeuchi, *Nat. Mater.* **2006**, *5*, 286.
[11] A. C. Fischer-Cripps, *Nanoindentation*, Springer, New York, NY **2004**.
[12] C. A. Schuh, *Mater. Today* **2006**, *9*, 32.

[13] X. G. Ma, K. Komvopoulos, *Appl. Phys. Lett.* **2004**, *84*, 4274.
[14] K. Komvopoulos, X. G. Ma, *Appl. Phys. Lett.* **2005**, *87*, 263108.
[15] C. P. Frick, T. W. Lang, K. Spark, K. Gall, *Acta Mater.* **2006**, *54*, 2223.
[16] T. Waitz, V. Kazykhanov, H. P. Karnthaler, *Acta Mater.* **2004**, *52*, 137.
[17] Y. Q. Fu, S. Zhang, M. J. Wu, W. M. Huang, H. J. Du, J. K. Luo, A. J. Flewitt, W. I. Milue, *Thin Solid Films* **2006**, *515*, 80.
[18] A. Ibarra, J. San Juan, E. H. Bocanegra, D. Caillard, M. L. Nó, *Mater. Sci. Eng. A* **2006**, *438–440*, 787.
[19] A. Ibarra, D. Caillard, J. San Juan, M. L. Nó, *Appl. Phys. Lett.* **2007**, *90*, 101907.
[20] V. Recarte, R. B. Perez-Saez, E. H. Bocanegra, M. L. Nó, J. San Juan, *Metall. Mater. Trans. A* **2002**, *33*, 2581.
[21] M. D. Uchic, D. M. Dimiduk, J. N. Florando, W. D. Nix, *Science* **2004**, *305*, 986.
[22] J. R. Greer, W. C. Oliver, W. D. Nix, *Acta Mater.* **2005**, *53*, 1821.
[23] H. Zhang, B. E. Schuster, Q. Wei, K. T. Ramesh, *Scr. Mater.* **2006**, *54*, 181.
[24] C. A. Schuh, J. K. Mason, A. C. Lund, *Nat. Mater.* **2005**, *4*, 617.
[25] A. Ibarra, J. San Juan, E. H. Bocanegra, M. L. Nó, *Acta Mater.* **2007**, *55*, 4789.
[26] H. Horikawa, S. Ichinoise, K. Morii, S. Miyazaki, K. Otsuka, *Metall. Trans. A* **1988**, *19*, 915.
[27] D. Xu, B. Cai, G. Ding, Y. Zhou, A. Yu, L. Wang, Z. Xiaolin, *Proc. Conf. on Electronics and Structures for MEMS*, SPIE, Bellingham, WA **1999**, Proc No. 3891, 369.
[28] H. J. Zhang, C. J. Qiu, *Mater. Sci. Eng. A* **2006**, *438–440*, 1106.
[29] A. Ishida, M. Sato, *Acta Mater.* **2003**, *51*, 5571.
[30] J. R. Greer, W. C. Oliver, W. D. Nix, *Acta Mater.* **2006**, *54*, 1705.

